AIAA'87

AIAA-87-0411
Viscous Transonic Flow Over Aero-Foils Using Transonic Full Potential Equation in a System of Cartesian Coordinates

S.S. Desai and R. Rangarajan,
National Aeronautical Laboratory,
Bangalore, India

AIAA 25th Aerospace Sciences Meeting
January 12-15, 1987/Reno, Nevada

VISCOUS TRANSONIC FLOW OVER AEROFOILS USING TRANSONIC FULL POTENTIAL EQUATION IN A SYSTEM OF CARTESIAN COORDINATES

S.S.Desai and R.Rangarajan
Scientists, Aerodynamics Division
National Aeronautical Laboratory
P.B.No.1779, BANGALORE-560 017, INDIA

ABSTRACT

Results are presented here for viscous transonic flow over aerofoils to demonstrate the capabilities of a code based on transonic full potential equation in a system of Cartesian coordinates. For this purpose a code based on Carlson's scheme utilizing Cartesian coordinates has been written incorporating many improvements apart from incidentally enhancing its computational efficiency. Thus the improvements in the numerical implementation of the surface boundary condition renders the code robust, resulting in an enhanced M-α domain in which accurate results can be obtained from the code. Further, Green's lag entrainment method is used along with transpiration model to include viscous effects due to aerofoil and wake. An empirical procedure is included to make the drag calculation more realistic. A viscous-ramp model is incorporated to enable cases of strong shock boundary layer interactions to be computed. The code has been validated extensively against experimental results.

1. INTRODUCTION

A variety of codes is known to be in existence to compute transonic flow over aerofoils. The, differ from one another in the form of the governing equation: full potential or small perturbation in conservative or non-conservative form, etc; in the choice of the coordinate system: conformal or general body-fitted coordinates, etc.; in the manner of application of the viscous corrections: integral or differential method of boundary layer calculations, displacement or transpiration model, direct or indirect mode of viscous coupling, etc.

Because of the availability of powerful digital computers one method has hardly any edge over another in terms of demand on computing resources. What therefore should distinguish any method over the rest is really the confidence with which the code can be used in its predictive role; such confidence can only be developed by extensive validation of the code against experiment.

In this paper results are obtained using a code written in a Cartesian system, a scheme pioneered by Carlson[1]. Though not favoured generally these days - with body-fitted coordinates in great vogue - a Cartesian system has, apart from its simplicity, several advantages, particularly regarding the ease with which 3-dimensional transonic codes can be devised[2,3]. The resulting 3-d codes would require less computing resources, a feature that compelled in the present context of our CFD work at NAL with less computing resources, much effort in 2-d transonic analysis with a Cartesian grid in order first to gain enough experience. This effort[4,5] culminated in reasonable sophistication in the code to predict transonic 2-d flows as well as to design aerofoils for given pressure distributions. Here results are presented for the analysis of transonic flow over aerofoils for the three cases specified for the Viscous Transonic Aerofoil Workshop being sponsored by the AIAA Fluid Dynamics Technical Committee and being organised by Terry L Holst. To bring out clearly the capability of the code a few additional cases, for which experimental data base exists, are also presented along with comparisons.

2. GOVERNING EQUATIONS AND THE BOUNDARY CONDITIONS

2.1 GOVERNING EQUATIONS

The full potential equation, in a stretched Cartesian grid $\xi = \xi(x)$, $\eta = \eta(y)$ is solved in the form:

$$(\tilde{a}^2-U^2)f(f\phi_\xi)_\xi - 2UVfg\phi_{\xi\eta} + (\tilde{a}^2-V^2)g(g\phi_\eta)=0$$

where:

$$\phi = M_\infty (x\cos\alpha + y\sin\alpha + \phi)$$

$$\tilde{a}=\frac{a}{a_\infty} = \left[1 - \frac{\gamma-1}{2}(U^2+V^2-M_\infty^2)\right]^{\frac{1}{2}}$$

$$U=M_\infty(\cos\alpha + f\phi_\xi) \ , \ V=M_\infty(\sin\alpha + g\phi_\eta)$$

$f=d\xi/dx$, $g=d\eta/dy$

a = Speed of sound

α = Angle of incidence

In the non-dimensionalization there is a slight departure here from Carlson: instead of q_∞, M_∞ appears in the non-dimensionalisation of ϕ, U and V.

2.2 BOUNDARY CONDITIONS

(a) Far-field Boundary Conditions:

The far-field corresponds to that of a single vortex of strength Γ placed at the origin of coordinates:

$$\phi \sim -\frac{\Gamma}{2\pi}\tan^{-1}[(1-M_\infty^2)^{\frac{1}{2}}\tan(\tan^{-1}\frac{y}{x} - \alpha)]$$

where Γ is the circulation consistent with the Kutta condition.

This boundary condition is applied at the edges of the computational domain that indeed correspond to the infinity of the physical domain as a result of the following (independent) stretchings of the x- and y- coordinates[1](see figure 1).

$$x = \pm x_4 + A_2\tan[\tfrac{\pi}{2}(\xi \mp \xi_4)] + A_3\tan[\tfrac{\pi}{2}(\xi \mp \xi_4)^3]$$

($\mp$ for $-\infty < x \le x_4$ and $x_4 \le x < \infty$ respectively)

$$= \xi\,(a + b\xi^2), \text{ for } -x_4 \le x \le x_4$$

$$y = A_1\tan(\tfrac{\pi}{2}\eta) \text{ for } -\infty < y < \infty$$

where following Carlson:

$A_1 = 0.246,\ A_2 = 0.15,\ A_3 = 3.87$

and normally $X_4 = 0.49,\ \xi_4 = 2$ are found to be well suited as seen from many numerical experiments. $X_4 = 0.49$ implies that both the leading edge and the trailing edge of the aerofoil are avoided as grid points, the first and the last y-grid lines being placed at 1% chord respectively from the leading and the trailing edges; $\xi_4 = 2$ implies that there are twice as many points on the aerofoil as there are outside of it.

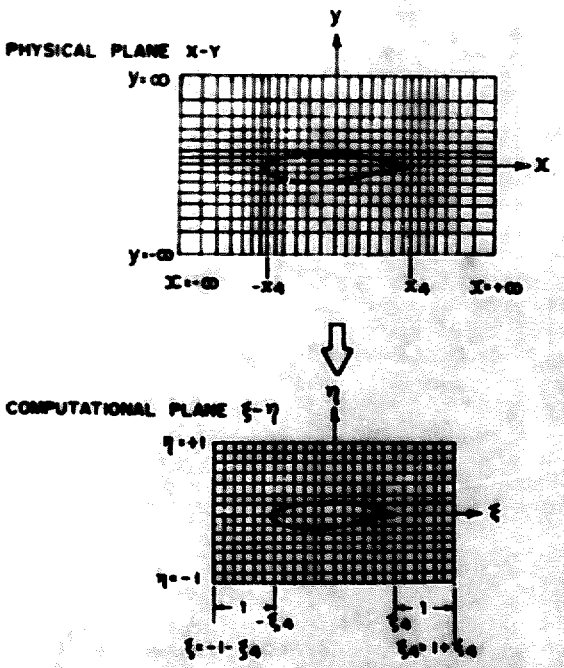

Fig.1 - SCHEMATIC OF COMPUTATIONAL AND THE PHYSICAL DOMAINS

(b) The Surface Boundary Condition:

A difficulty arises in the surface boundary condition for a Cartesian system because the intersections between the body and the grid lines are not necessarily the grid points. The surface tangency condition $\vec{q}\cdot\vec{n} = 0$ can only be satisfied using a Taylor series approximation around the first grid point in the flow domain outside the body. The application of the surface tangency condition then determines a value for the potential ϕ at the first "dummy point" within the body (see figure 2). It may be mentioned here that the determination of this dummy value is a simple matter when the coordinate system is body-fitted and orthogonal $\partial\phi/\partial n = 0$ could then mean that the value of ϕ at the first dummy is the same as that at the first field point.

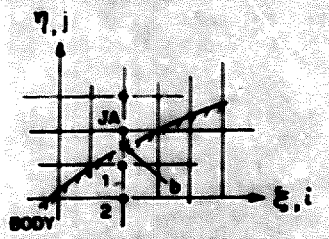

1,2 : DUMMY POINTS
JA: FIRST FIELD POINT
b : BODY POINT

Fig.2 - APPLICATION OF SURFACE TANGENCY IN CARTESIAN GRID

Another difficulty, a source of instability, arises whenever the flow at the first field point happens to be supersonic and the v-component of velocity has the direction from inside to the outside ($V > 0$ for upper and $V < 0$ for lower surfaces). This is necessary while using rotated type dependent differencing of the governing equations. Carlson[1] takes a linear extrapolation for this second dummy value:

$$\phi_2 = -\phi_{JA} + 2\phi_1$$

This linear extrapolation is the main source of instability problem in Carlson's code, restricting severely the M-α working domain of the code.

Actually, linear extrapolation implies that $\phi_{\eta\eta} = 0$ at JA in a backward differencing that is used while applying a rotated differencing scheme at the field point JA. While still using a linear

extrapolation, we avoid the instability by a compensative addition of the second derivative $\phi_{\eta\eta}$ now as calculated by a centred differencing, at JA:

$$\phi_{\eta\eta}|_{JA} = \frac{\phi_{JA+1} - 2\,\phi_{JA} + \phi_{1}}{(\Delta\eta)^2}$$

This change has improved the stability and has enhanced the working M-α domain of the code.

3. ROTATED TYPE-DIFFERENCING AND THE SUCCESSIVE LINE OVER- RELAXATION

The features such as rotated type-differencing of the governing differential equation in streamline coordinate form, the addition of explicit ϕ_{st} terms (s, streamwise coordinate; t, the pseudo-time) for the stability of the scheme, the evolution of the ϕ field from zero in a successive line over relaxation, with sweep in ξ-direction and a tridiagonal solution in η-direction, are all identical to those of Carlson and are not covered here in detail. See also Jameson[6] for aspects of the stability arguments.

4. VISCOUS CORRECTIONS

Boundary layer and wake parameters for a given pressure distribution, obtained during potential flow solution, are computed following the method of Green et al. A fourth-order Runge-Kutta scheme is used to integrate the two integral boundary layer equations together with an integral turbulent kinetic energy equation (Desai and Kiske[7]). The integration is done starting from a given transition point with an assumed initial value of θ/c, the momentum thickness (normally 0.0002 for aerofoil with natural transition). The initial values for the remaining parameters - H, shape factor, and C_E, entrainment coefficient, can be obtained either with an assumption of flat-plate boundary layer or an equilibrium boundary layer at the initial point. For most of the calculations we use the option of an equilibrium boundary layer. The wake parameters are obtained for upper and lower portions separately, continuing the integration of the three integral equations holding $c_f = 0$ and with the values of the momentum thickness and shape factor for the upper and lower surfaces at the trailing edge as the initial value for wake. Actually the trailing edge is not a point where boundary layer calculations are made; the values here are extrapolated from two values of θ upstream of the trailing edge point. For the initial values of the remaining parameter, C_E during wake calculation, again an assumption of equilibrium is made. To make the boundary layer integrations accurate, the interval between the last grid point near the trailing edge and the point where the boundary layer computations begin are divided into 65 points. The pressure coefficients at these points are obtained by spline interpolations from the values at the grid points of the potential calculation. Similarly the wake region behind the trailing edge, upto the last x-grid, is divided into 35 points with spline interpolation for the pressure coefficients.

From the computed boundary layer displacement thickness and the potential values of ρ, the density and u, the streamwise velocity component, transpiration velocity is calculated:

$$V_n = \frac{1}{\rho}\frac{d}{ds}(\rho u \delta^*)$$

by using smoothed values of δ^* and a spline routine. For the wake region the transpiration corresponds to a jump in normal velocity

$$\Delta V = \frac{1}{\rho_w}\frac{d}{ds}(\rho_w\, u_w\, \delta_w^*)$$

where the suffix w denotes wake quantities and δ_w^* is the sum of the upper and lower portions of the wake:

$$\delta_w^* = \delta_{w\,\text{upper}}^* + \delta_{w\,\text{lower}}^*$$

Finally, wake curvature effects are accounted for by allowing a jump in tangential velocity, Δu, across the wake cut (see Lock[8] for details).

$$\Delta u = -ku\,(\delta_w^* + \theta_w)$$

where K = wake curvature

In the implementation it is useful to consider this as a change in circulation along the wake-cut over a distance Δx:

$$\Delta\Gamma_{wake} = \Delta u.\,\Delta x$$

The procedure of viscous correction is schematically shown in figure 3.

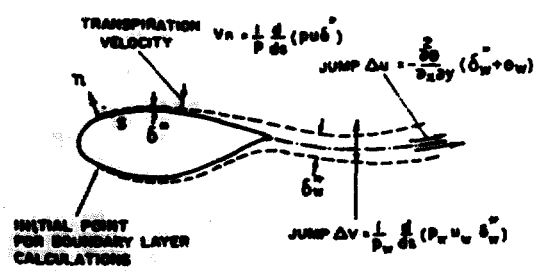

Fig.3 - SCHEMATIC SKETCH FOR THE VISCOUS CORRECTION

5. VISCOUS RAMP MODEL FOR THE SIMULATION OF STRONG SHOCK BOUNDARY LAYER INTERACTION

To simulate the sudden thickening of the boundary layer behind a strong shock we place a certain viscous ramp at the foot of the shock whenever the shock upstream Mach number exceeds 1.25. For the ramp thickness δ_R we use the empirical formula of Lee, Thomas and Holst[9] (see figure 4):

$$\delta_R(s)/c = 0 \text{ , for } S<S_{sh} \quad (S_{sh} = \text{shock location})$$

$$= \beta_1 \theta_{max}\{1 - \exp[(S_{sh} - S)/c\beta_1]\}$$

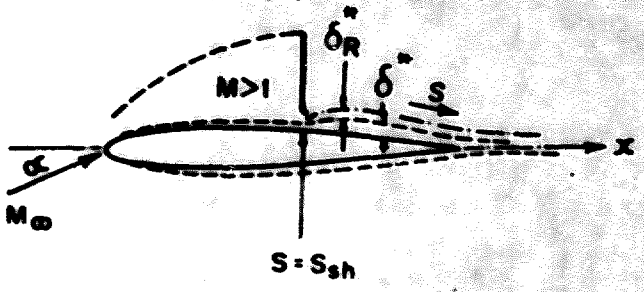

Fig.4 - VISCOUS RAMP FOR THE STRONG VISCOUS - INVISCID INTERACTION

where β_1 is a constant. We take this equal to 0.5 for all cases. θ_{max} in the above expression represents maximum deflection angle for an attached shock for a given shock upstream Mach number which is determined by the potential solution. Since we are normally interested in shock Mach numbers between 1.2 and 1.6, it is approximated as:

$$\theta_{max} = \pi \cdot (25(M_1 - 1.2) + 4)/180 \text{ radians}$$

Here M_1 is the shock upstream Mach number. This linear formula implies $\theta_{max} = 4°$ for $M_1 = 1.2$ and $\theta_{max} = 14°$ for $M_1 = 1.6$

The effective δ^* including the viscous ramp is given by

$$\delta^*_{eff} = \delta^*, \text{ for } s < s_{sh}$$

$$= (\delta^* + \delta^*_R)/2, \text{ for } s \geq s_{sh}$$

The appropriate transpiration velocities are obtained from this effective displacement thickness.

6. SOME NUMERICAL ASPECTS OF THE CODE

(a) Grid Sequencing:

The solution is advanced in three grids, with a zero field in the crude grid:

Crude grid : M x N
Medium grid : (2M-1) x (2N-1)
Fine grid : (4M-3) x (4N-3)

It is also possible to perform calculations on a very fine grid (8M-7) x (8N-7). But this is not used in routine calculations; three grid levels are already found to give adequate results. Normally, and also for the calculations presented here,

M = 13, N = 7

(b) Convergence Criterion:

The calculations are terminated in the fine grid as soon as the maximum spatial difference in ϕ for two successive iterations becomes less than or equal to a small quantity δ. (δ = 0.00001 normally, and also for all the results presented here)

This criterion is not followed in the first two grid levels; in the crude grid only 50 iterations are done without any check for convergence; in the medium grid the process is terminated when the successive spatial ϕ difference is less than or equal to 10 δ.

Typical convergence history is shown in figure 5.

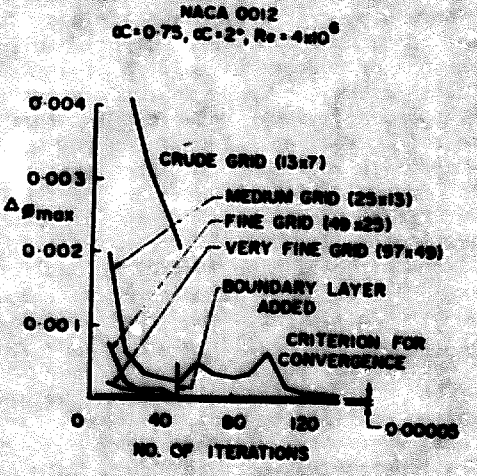

Fig.5 - TYPICAL CONVERGENCE PATTERN

Failure to converge is usually detected by monitoring the square of the speed of sound becoming negative and the process comes to a halt.

(c) Viscous Corrections:

No viscous corrections are made during the 50 crude grid iterations. In the medium grid viscous calculations are first started as soon as one of the two conditions is satisfied: maximum spatial difference in ϕ between the successive iterations is less than 50 δ or 50 inviscid iterations. Thereafter viscous calculations are done after every 10 inviscid iterations. In the

fine grid the viscous corrections are started at the earlier of the two conditions: 50 inviscid iterations or maximum successive spatial difference in ϕ is less than 10δ. Thereafter, viscous updating is followed after every 10 inviscid iterations.

(d) Computer Requirements:

The code is written in standard Fortran for the NAL's UNIVAC 1100/60-C computer, capable of an estimated 0.3 MFLOPS. The code requires 39K words of storage and takes between 1 to 4 minutes of CPU time. The final pressure distribution and the boundary layer and wake parameters can be plotted out on a Calcomp plotter.

(e) Working M- α Domain of the Code:

Typical working domain of the code can be illustrated by figure 6 which pertains to a NACA 0012 aerofoil. Roughly speaking the code fails to converge whenever shock upstream Mach number exceeds 1.4 which invariably signifies massive shock-induced separation behind the foot of the shock.

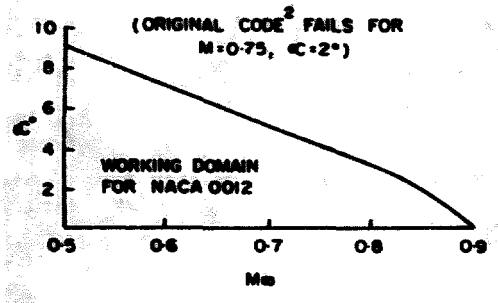

Fig.6 - DOMAIN OF THE PRESENT CODE

7. RESULTS AND DISCUSSIONS

Before proceeding with the presentation of viscous results, we should note here the capability of Carlson's code (of which the present work is a refinement) in its inviscid mode.

In the GAMM Workshop[10] on inviscid transonic computations this method emerged as the one that give results falling midway in the scatter of data obtained by different Euler solutions, Figure 7. Figure 7 also shows three cases where inviscid calculations by the present NAL code are compared with the Euler calculations of Rizzi. Remarkable overall agreement in all the three cases is noteworthy.

Next, figure 8 gives a comparison between experiments (Cook[11]) and computations for RAE 2814 and figures 9-10 for RAE 2815. The comparison for the pressure distributions as well as for the boundary layer parameters is very good.

Figures 11-20 pertain to the NACA 0012 aerofoil for which considerable experimental data is available in open literature. Here comparisons are made with the experiments of Harris[12]. For comparison with these results correction of $\Delta\alpha = -1.55\ C_L$ in degrees to the geometric incidence, α_g, has been adopted as suggested in Reference 12. The computations are done for a Reynolds number of 9×10^6 with the location of transition fixed at 5% of chord.

Figure 11 shows the comparison of pressure distribution with experiments for $M_\infty = 0.7$, $\alpha_g = 1.86^\circ$, for this mildly supercritical case the comparison is reasonably good. Figure 12 shows the case of a strong shock for $M_\infty = 0.80$ and $\alpha_g = 1.86^\circ$. The comparison for an α of 1.55° is extremely good for both the upper and the lower surfaces. Figures 13-15 bring out comparison of pressure distributions under conditions which almost correspond to the experimentally observed stall point. While figures 13 and 14 show cases of lor freestream Mach numbers 0.55 and 0.60 respectively, figure 15 shows the case of stall for a moderate Mach number of 0.7 and $\alpha_g = 5.86$. Figure 16 shows comparisons for a Mach number of 0.74 and $\alpha_g = 4.86^\circ$ at which strong shock prevails. While we see a good comparison in all cases for the lower surface. there are certain differences for the upper surface. For $M_\infty = 0.55$, $\alpha_g = 9.86^\circ$ and for $M_\infty = 06$ and $\alpha_g = 8.86^\circ$, there are discrepancies in the pressure peak occurring within the first 10%of chord of the aerofoil and also behind the nose shock position. The position of nose shock however is well predicted. Similarly there is a good comparison for the shock position in figures 15 and 16. There are differences downstream of the shock, however. While the discrepancies in the peak values near the nose portion could be linked to the crude grid structure around the nose region. the discrepancies downstream of the shock appear to be due to the viscous rawp model, which may require refinements around the stall conditions. The viscous-ramp seems to work reasonably well even for conditions slightly below the stall. For such a case with $M_\infty = 0.80$, $\alpha_g = 2.86$, comparisons are shown between experiments and inviscid and viscous calculations, with and without viscous ramp, Figure 17. As can be seen the viscous ramp seems to represent the sudden thickening of the boundary layer at the foot of the shock very well; the simulation of strong shock boundary layer interaction is rather good.

Figure 18 shows the shock location vs Mach number for the NACA 0012 at zero incidence. The comparison is very good upto a freestream Mach number of 0.85.

Figures 19 and 20 give a comparison of drag with experiments. Figure 19 shows the comparison for the zero-lift drag and figure 20 shows comparison of drag rise for a freestream Mach number of 0.7. The comparison for drag reveals only modest agreement.

Figure 21 shows the comparison for C_L vs α curve for a Mach number of 0.7. The correction to the geometric incidence turns out to be $\Delta\alpha = -1.90\ C_L$ as against $\Delta\alpha = -1.55\ C_L$ suggested by Harris based on the analysis of Barnwell[13].

Figures 22 to 26 pertain to the RAE 2822 for which experimental data base exists[14]. Figure 22 gives a comparison for $M_\infty = 0.725$ and $\alpha_g = 2.92$ (Case 6 of AGARD 138). Here computations were made to adjust the C_L. There are slight differences at the shock on the upper surface and between 10% and 50% on the lower surface. In the experiments there is a sharp local hump in the pressure distribution at about 5% on the upper surface which can be attributed to the localised effect of the boundary layer transition trip. Overall agreement for C_L and for the coefficients C_L, C_D, C_m is fairly good. Figure 23 shows a good comparison between the displacement thickness and the skin friction on the upper surface for this case.

Figure 24 compares the pressure distributions for $M_\infty = 0.75$, $\alpha_g = 3.19$ (Case 10 of AGARD AR 138). This is a case where one observed separation behind the foot of the shock. As can be seen, while the viscous ramp has improved the comparison of C_L behind the foot of the shock, the shock position comparison has deteriorated. There is a slight overall disagreement of C_p for the lower surface. The localised hump due to the transition strip is more pronounced here. Comparison for the upper surface displacement thickness and skin friction is given in figure 25. The comparison for the displacement thickness behind the shock is only modest, but shows a considerable improvement over that without the ramp. There are not enough experimental data for the skin friction comparison, but differences due to the ramp can be clearly seen.

Figure 26 shows the sonic line for this case.

Finally, figures 27 to 3 present the results for the Jones aerofoil suggested as a "blind" case for evaluating the different transonic viscous codes for analysing flow over aerofoils.

Table 1 gives the details of the CPU time and convergence for the critical Test cases, marked (***).

8. CONCLUSION

In summary, the following observations can be made based on the presentations made here.

i) an efficient code has resulted in the use of a stretched Cartesian grid system for the analysis of transonic full potential equation in non-conservative form

ii) the viscous corrections for boundary layer and wake, including wake curvature effects, are demonstrated to be effective

iii) the code performs well in the absence of strong shocks with shock upstream Mach numbers less than 1.4

iv) with the inclusion of a viscous ramp the code is able to handle cases of strong shock with small separation at the foot of the shock

v) an empirical drag correction method is introduced in the code which yields realistic, though not very accurate drag values.

REFERENCES

01. CARLSON,L.A.: Transonic analysis and design using Cartesian coordinates, J.Aircraft, Vol.13, No.5, PP 342-356, 1976.

02. DESAI,S.S.,RANGARAJAN,R., RAVICHANDRAN,K.S.: A preliminary note on the development of a three-dimensional potential code in Cartesian coordinates, NAL TM AE 8504, 1985.

03. BOPPE,C.W.: Transonic flow field analysis for wing fuselage configurations, NASA CR 3243, May 1980.

04. RANGARAJAN,R., DESAI,S.S., RAMASWAMY,M.A.: 2-D Transonic analysis and design program in Cartesian coordinates (TRADE-1), NAL AE-TM-6-83, September 1983.

05. RANGARAJAN,R.: Analysis and design of supercritical aerofoils, M.Sc Thesis, Dept. of Aeronautical Engineering, Indian Institute of Science, Bangalore, January 1986.

06. JAMESON,A.: Iterative solution of transonic flows over aerofoils and wings, including flows at Mach 1, Communications on Pure and Applied Mathematics, Vol.27, PP 283-309, 1974.

07. DESAI,S.S., KISKE,S.: A computer program to calculate turbulent boundary layers and wakes in compressible flow with arbitrary pressure gradient based on Green's Lag-entrainment method, Bericht Nr. 89/1982, Institut für Thermo- u.Fluiddynamik, Ruhr University Bochum, 1982.

08. LOCK,R.C.: Calculation of viscous effects on aerofoils in compressible flow, RAE Tech Memo, Aero 1646, September 1975.

09. LEE,S.C., THOMAS,S.D., HOLST,T.L.: A fast viscous correction method for full-potential transonic wing analysis, ICAS-84-1.2.3, Vol.1, Toulouse, France, Sept. 1984.

10. VIVIAND,H., RIZZI,A.(Eds): Notes on numerical fluid mechanics, Vol.3 - Proceedings of the GAMM Workshop on Numerical methods for the computation of inviscid transonic flows with shock waves, 1981.

11. COOK,T.A.: Measurements of the boundary layers and wake of two aerofoil sections at high Reynolds numbers end high-subsonic numbers, ARC R&M No.3722, June 1971.

12. HARRIS,C.D.: Two-dimensional aerodynamic characteristics of the NACA 0012 aerofoil in the Langley 8-foot transonic pressure tunnel, NASA TM 81927, April 1981.

13. BARNWELL,R.W.: Design and performance evaluation of slotted wall for 2-d wind tunnels, NASA TM-78648, February 1978.

14. COOK,P.H., Mc DONALD,M.A., FIRMIN, M.C.P.: Aerofoil RAE 2822 Pressure distributions and boundary layer and wake measurements, A6-1, A6-57, Agard AR-138, 'Experimental Data Base for Computer Program Assessment," May 1979.

ACKNOWLEDGEMENTS

We take this opportunity to thank Prof.R. Narasimha, Director. National Aeronautical Laboratory for the encouragement in our work. The earlier stage of this work was done under an AR&DB grant from the Aeronautical Research and Development Board. We acknowledge the help from Mr.S.Viswanathan in plotting work and from Ms M.Manjula in the patient typing of the paper.

Table 1. DETAILS OF CRITICAL TEST CASES

AEROFOIL	FREESTREAM	CRUDE (13x 7)	MEDIUM (25x13)	FINE (49x25)	CPU (SECS)	CONV RATIO
		NO. OF ITERATIONS				
NACA 0012	M = 0.55 α = 8.34°	50	150	220	191	0.0026
NACA 0012	M = 0.80 α = 2.26°	50	150	225	197	0.0021
RAE 2822	M = 0.75 α = 3.19°	50	160	450	345	0.0009
JONES	M = 0.75 α = 2.00°	50	102	450	334	0.0031
COMPUTER STORAGE		39K WORDS (UNIVAC 1100/81-HS)			RATIO OF RESIDUE FINAL TO RESIDUE 1ST ITER	

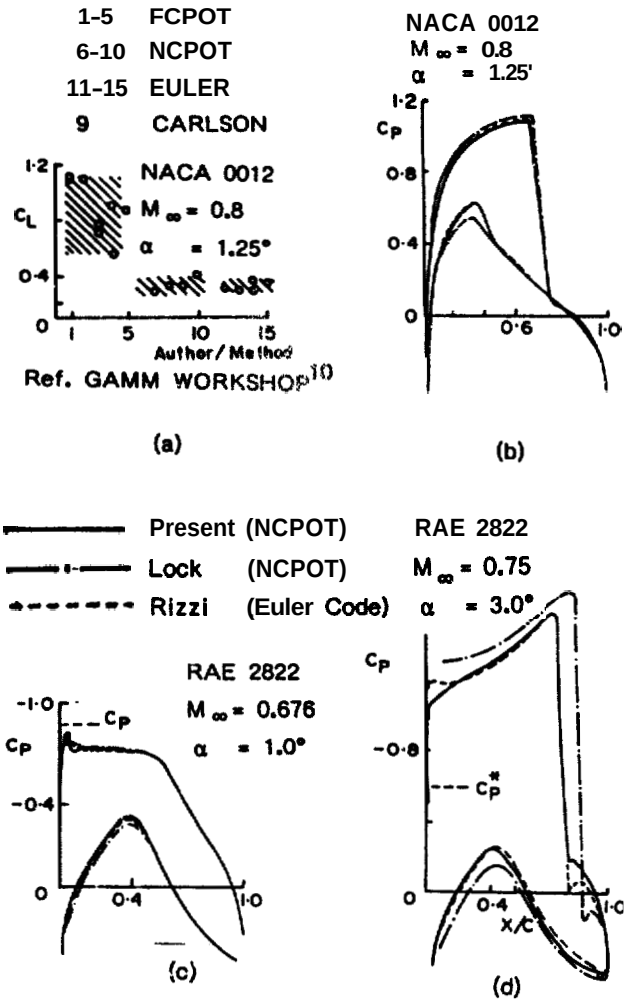

Fig.7 COMPARISON OF INVISCID RESULTS FROM DIFFERENT THEORIES

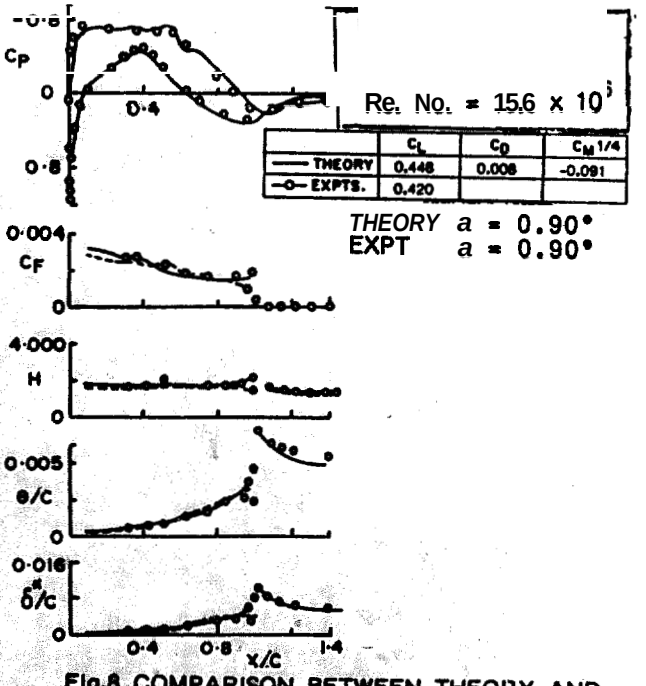

	C_L	C_D	$C_{M\,1/4}$
THEORY	0.448	0.008	-0.091
EXPTS.	0.420		

Fig.8 COMPARISON BETWEEN THEORY AND EXPERIMENT

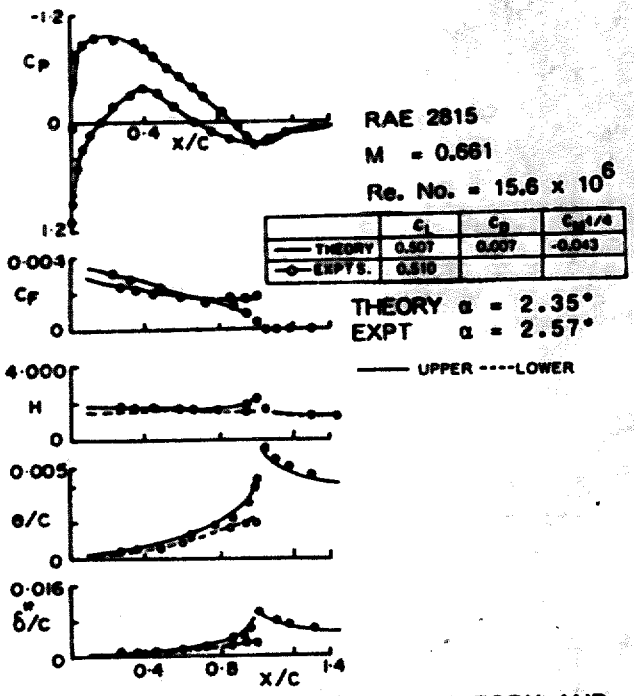

Fig.9 COMPARISON BETWEEN THEORY AND EXPERIMENT

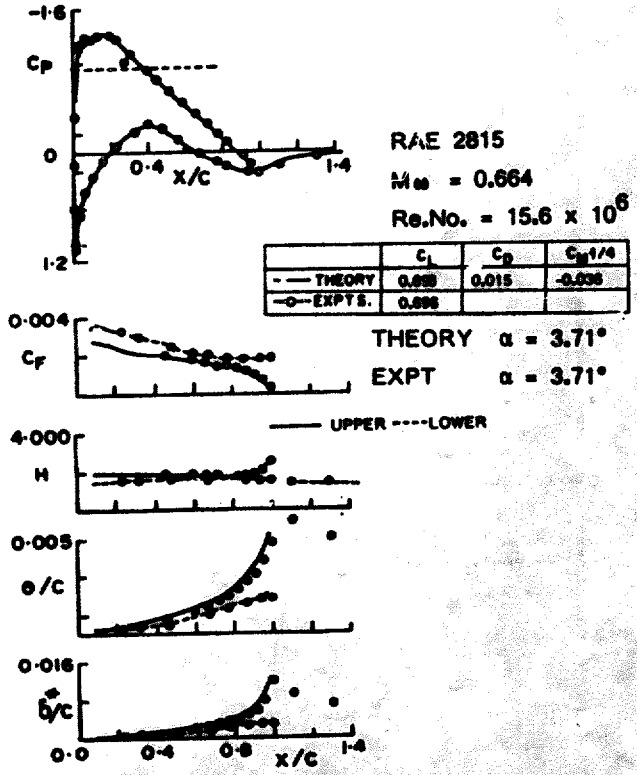

Fig.10 COMPARISON BETWEEN THEORY AND EXPERIMENT

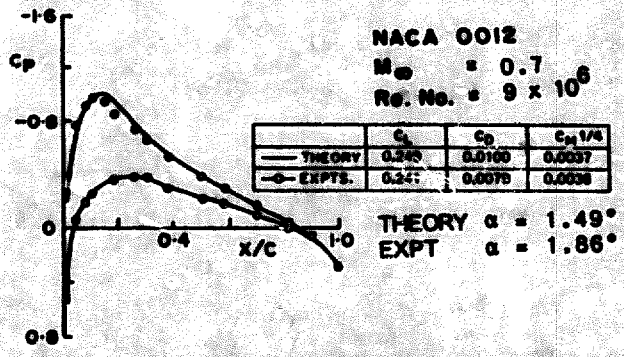

Fig.11 COMPARISON BETWEEN THEORY AND EXPERIMENT

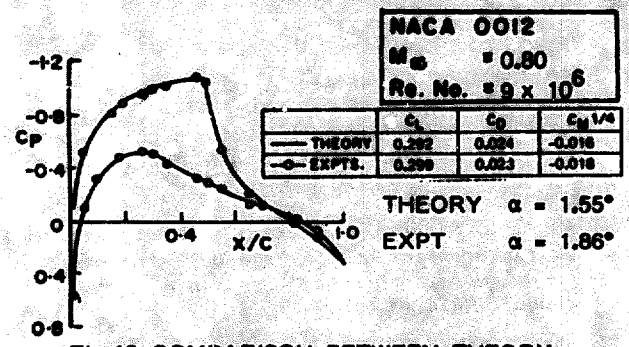

Fig.12 COMPARISON BETWEEN THEORY AND EXPERIMENT

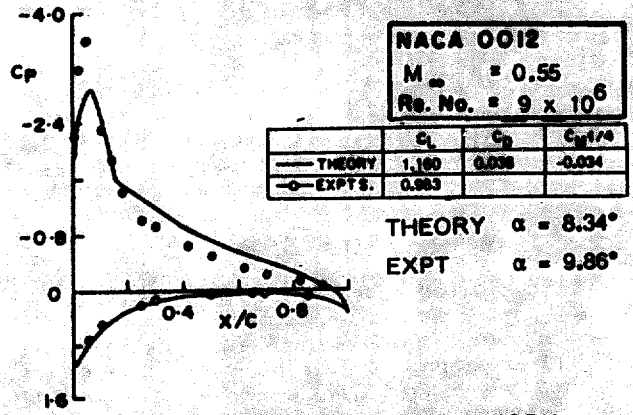

Fig.13 COMPARISON BETWEEN THEORY AND EXPERIMENT

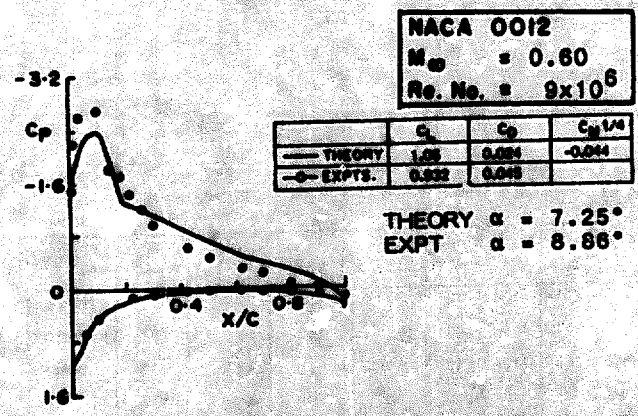

Fig.14 COMPARISON BETWEEN THEORY AND EXPERIMENT

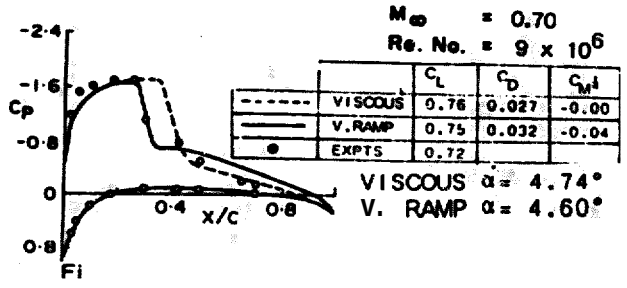

		C_L	C_D	$C_{M\frac{1}{4}}$
------	VISCOUS	0.76	0.027	-0.00
———	V.RAMP	0.75	0.032	-0.04
●	EXPTS	0.72		

Fi

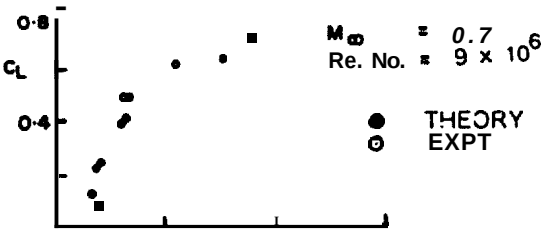

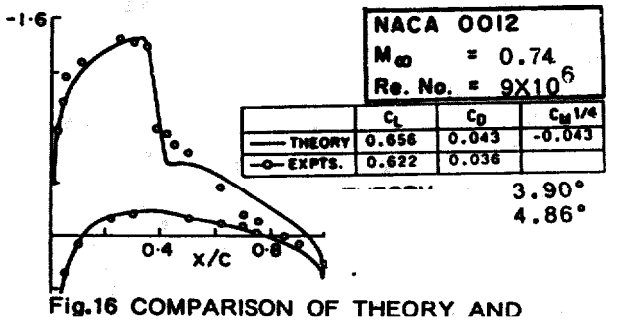

	C_L	C_D	$C_{M\,1/4}$
—— THEORY	0.656	0.043	-0.043
—o— EXPTS.	0.622	0.036	

Fig.16 COMPARISON OF THEORY AND

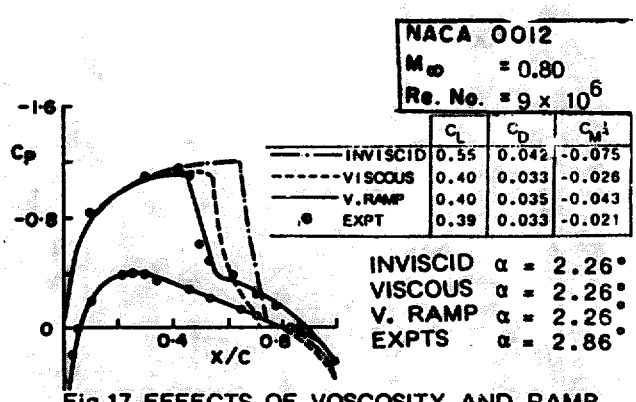

	C_L	C_D	$C_{M\frac{1}{4}}$
—·— INVISCID	0.55	0.042	-0.075
------ VISCOUS	0.40	0.033	-0.026
——— V.RAMP	0.40	0.035	-0.043
● EXPT	0.39	0.033	-0.021

Fig.17 EFFECTS OF VOSCOSITY AND RAMP MODEL FOR MARGINAL SEPARATION ON SHOCK LOCATION

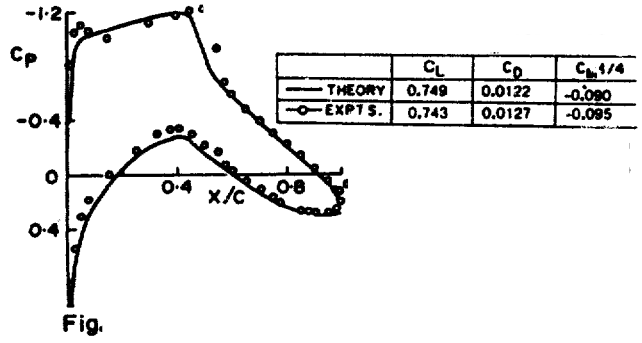

	C_L	C_D	$C_{M\,1/4}$
—— THEORY	0.749	0.0122	-0.090
—o— EXPTS.	0.743	0.0127	-0.095

Fig.

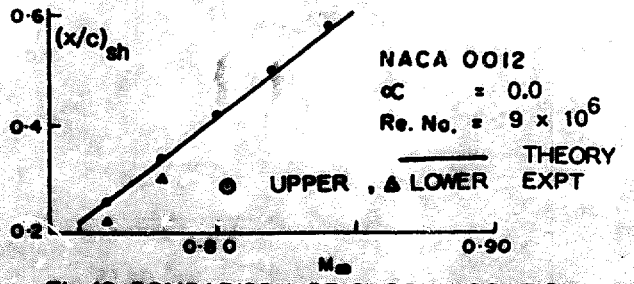

Fig.18 COMPARISON OF SHOCK LOCATION

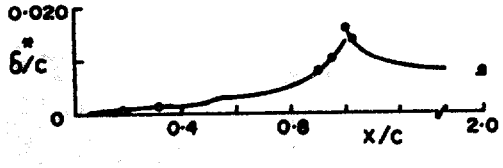

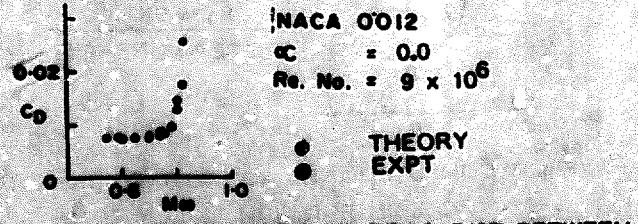

Fig.19 COMPARISON OF DRAG RISE BETWEEN THEORY AND EXPERIMENT

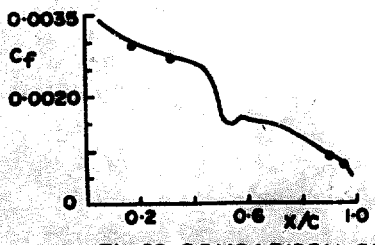

Fig.23 COMPARISON OF [illegible] THICKNESS AND SKIN FRICTION JONES AEROFOIL

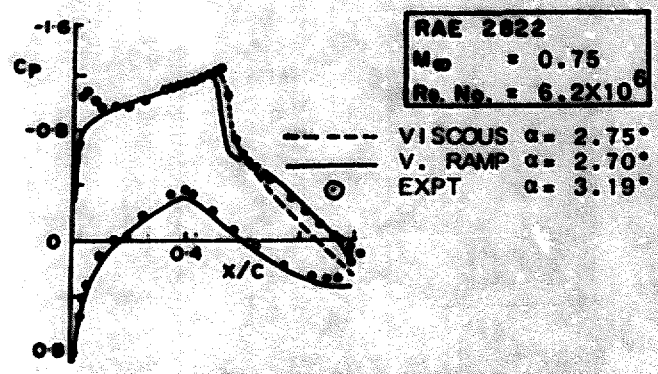

Fig.24 COMPARISON OF PRESSURE DISTRIBUTION BETWEEN THEORY AND EXPERIMENT

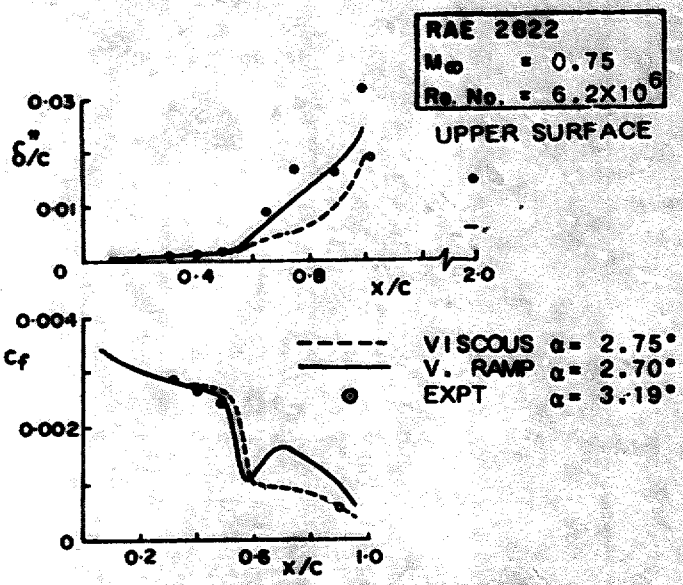

Fig.25 COMPARISON OF DISPLACEMENT THICKNESS AND SKIN FRICTION

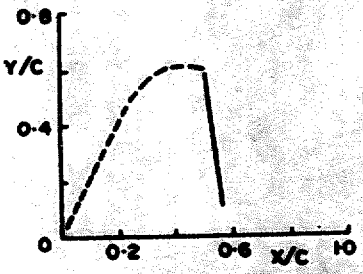

Fig.26 SONIC LINE ON THE UPPER SURFACE OF RAE 2822

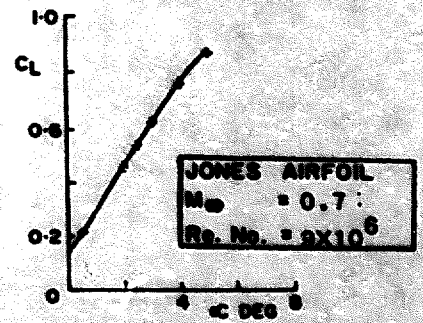

Fig.27 COMPUTED LIFT CURVE JONES AEROFOIL

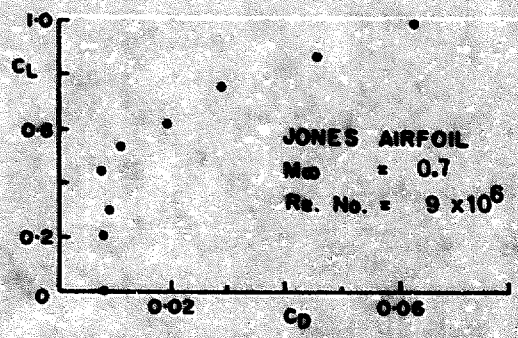

Fig.28 COMPUTED DRAG CURVE JONES AEROFOIL

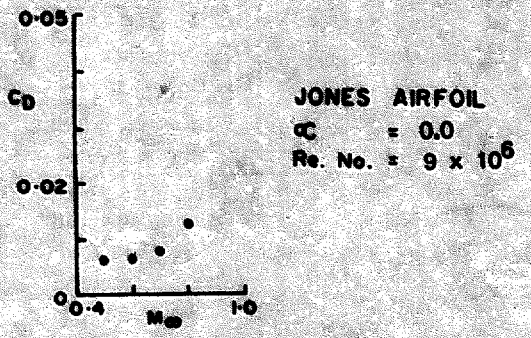

Fig.29 COMPUTED DRAG RISE JONES AEROFOIL

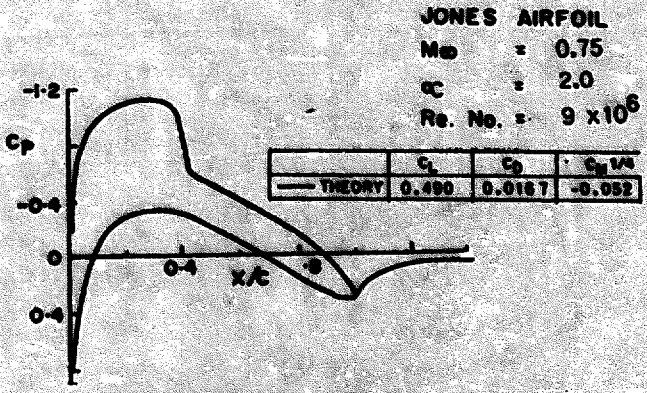

Fig.30 COMPUTED PRESSURE DISTRIBUTION JONES AEROFOIL

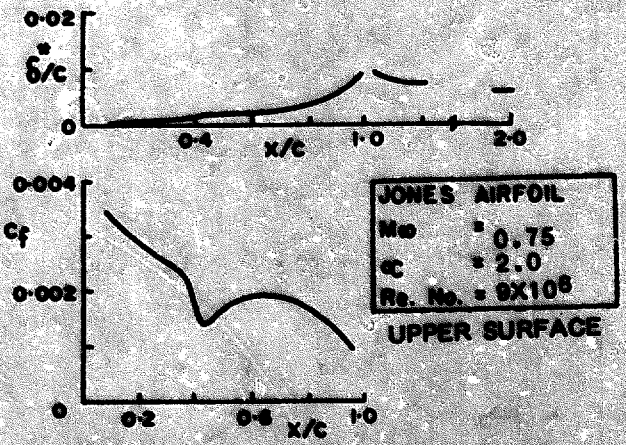

Fig.31 COMPUTED DISPLACEMENT THICKNESS AND SKIN FRICTION

AIAA'87

AIAA-87-0411
Viscous Transonic Flow Over Aero-Foils Using Transonic Full Potential Equation in a System of Cartesian Coordinates

S.S. Desai and R. Rangarajan,
National Aeronautical Laboratory,
Bangalore, India

AIAA 25th Aerospace Sciences Meeting
January 12-15, 1987/Reno, Nevada